Sensors and Actuators A 201 (2013) 352–356

Contents lists available at ScienceDirect

Sensors and Actuators A: Physical

journal homepage: www.elsevier.com/locate/sna

# Bent optical fiber taper for refractive index detection with a high sensitivity

Guigen Liu[a], Kaiwei Li[a,b], Peng Hao[a], Wenchao Zhou[a,b], Yihui Wu[a,*], Ming Xuan[a]

[a] State Key Laboratory of Applied Optics, Changchun Institute of Optics, Fine Mechanics and Physics, Chinese Academy of Sciences, Changchun 130033, China
[b] University of Chinese Academy of Sciences, Beijing 100039, China

ARTICLE INFO

*Article history:*
Received 19 March 2013
Received in revised form 18 June 2013
Accepted 31 July 2013
Available online 11 August 2013

*Keywords:*
Fiber-optic sensor
Bent optical fiber taper
Whispering gallery mode

ABSTRACT

A bent optical fiber taper (BOFT) is proposed for refractive index (RI) detection with a high sensitivity. The BOFT consists of a bent cladding downtaper where the whispering gallery mode (WGM) forms along the curved cladding-external medium interface due to radiation from the bent core. The phase change upon total internal reflection (TIR) of the WGM is a function of external RI, which is utilized for RI sensing. The incident angle of the TIR is decreased due to the tapered cladding, which speeds up the phase change and thus enhances the sensitivity. A high sensitivity of 4000 nm/RIU (RI unit) was experimentally obtained over a RI range of 1.424–1.435.



## 1. Introduction

The determination of refractive index (RI) is very important for a variety of practical applications, such as chemical, biological and pharmaceutical industries. Among various techniques for RI sensing, optical fiber based refractometers stand out due to their unique advantages, such as compact footprint, immunity to electromagnetic interference, capability of performing remote sensing, and multiplexing detection in a single device [1–8]. Specific fiber-optic refractometer configurations include optical fiber coil resonator [1], cladding-mode fiber Bragg grating [2,3], single-mode-multimode-single-mode (SMS) structure [4,5], microfiber embedded beside a microchannel [6], end-of-fiber Fabry–Perot tip [7], and tapered fiber modified by nanospheres [8], etc. In 2011, an improved SMS sensor using tapered fiber was proposed and reported to have a high sensitivity of 1900 nm/RIU (RI unit) or a resolution of $5.23 \times 10^{-6}$ RIU [9], which was believed by its authors to be the highest sensitivity obtained by an all-fiber-based RI sensor by then. Shortly after that, the sensitivity was further enhanced to 2735 nm/RIU by a twisted microfiber [10], and recently a tapered fiber mode interferometer was reported to have a RI resolution of $3.7 \times 10^{-6}$ RIU [11].

In this paper, we proposed a bent optical fiber taper (BOFT) (see Fig. 1) for RI detection with a high sensitivity of 4000 nm/RIU or a resolution of $2.5 \times 10^{-6}$ RIU assuming the same wavelength shift of 10 pm can be resolved as [11]. The feasibility of this BOFT for RI detection lies in a bent downtaper which consists of a tapered cladding and uniform core. Although the bending effects on uniform optical fibers have been investigated for decades [12–16] and some practical applications have been reported [17–23], all of them were devoted to bent fibers without cladding or with uniform cladding (or multiple uniform claddings). Furthermore, only a few papers on bent fiber-based refractometer have appeared [21–23], the main reasons are believed to be the poor spectral shapes of the resonance arising from whispering gallery mode (WGM) formed in the bent cladded fiber, significant background loss, weak oscillation patterns, and lack of good control method [23]. Therefore, the author of [23] revisited the resonance between cladding WGM and core mode and devised a cladding-thinned bent optical fiber to intensify the resonance oscillations for temperature and RI sensing. However, the BOFT proposed in this paper has a much better performance than the sensitivity of −866 nm/RIU for the bent cladding-thinned uniform fiber investigated in [23] and the RI resolution of $5.75 \times 10^{-5}$ RIU for a macrobending loss based fiber-optic refractometer reported in [21].

Most recently, a Mach–Zehnder interferometer based on an S-tapered fiber is proposed for refractive index sensing with a sensitivity reaching 2124 nm/RIU [24,25]. Bending of the taper gives birth to cladding modes which are highly dependent on the surrounding RIs. Although the effect of bending and tapering on sensitivity has been experimentally reported [25], no physical insights into how the bending and tapering contributes to the

* Corresponding author. Tel.: +86 431 86176915, fax: +86 431 5690271.
*E-mail addresses:* guigenliu@hotmail.com (G. Liu), likaiwei11@163.com (K. Li), hp312@126.com (P. Hao), zhouwenchao666@126.com (W. Zhou), yihuiwu@ciomp.ac.cn, ciomp_yihuiwu@hotmail.com (Y. Wu), xuanm@ciomp.ac.cn (M. Xuan).

0924-4247/$ – see front matter © 2013 Elsevier B.V. All rights reserved.
http://dx.doi.org/10.1016/j.sna.2013.07.041

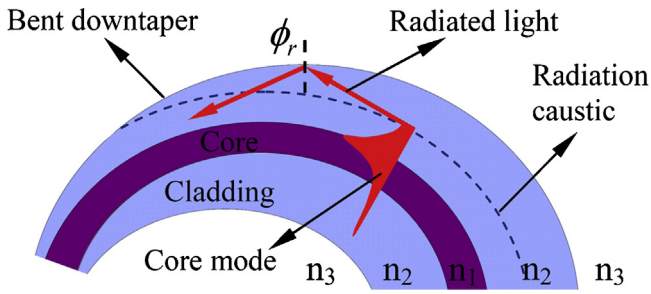


**Fig. 1.** Schematic showing the core mode and caustic radiation within the bent downtaper.

sensitivity enhancement have been illustrated. In this paper, we will clearly reveal the role of bending and tapering in improving the sensitivity.

## 2. Theory

### 2.1. Working principle

As shown in Fig. 1, when optical wave propagates through a bent fiber, caustic radiation occurs where the angular phase velocity of the evanescent field equals the light velocity in the cladding, the radiated light forms whispering gallery modes (WGMs) along the cladding-external medium wall by total internal reflection (TIR) [13–15]. The coupling between core mode and WGMs contributes to the oscillatory transmitted spectrum which contains a series of peaks and troughs. There is a phase change for the reflected wave after the TIR, the peak wavelengths shift while the phase change varies. The phase change is a function of surrounding RI, therefore, the peak wavelengths are dependent on surrounding RI, which comprises the working principle for the RI sensors based on BOFT. In the presence of a bent downtaper, the tapered cladding will enhance the sensitivity for RI detection since it decreases the incident angle of TIR and thus increases the phase change and wavelength shifts as surrounding RI varies.

### 2.2. Model

In order to model the bent downtaper, the denotations of some parameters are shown in Fig. 2(a). The polar coordinate is used to facilitate modeling. The taper before bending is assumed to be linear, so the dependence of the outer radius $r$ on the polar angle $\varphi$ after bending is also linear and given as

$$r = R + r_{cl} - R\varphi \tan\gamma \left(0 \le \varphi \le \frac{r_{cl} - r_w}{R\tan\gamma}\right) \tag{1}$$

where $R$, $r_{cl}$, $r_w$, and $\gamma$ are bend radius, starting cladding radius, waist radius, and half taper angle before bending, respectively. The radiation starts from point A, and is then reflected at point B on the cladding-external medium interface, after which the radiated ray recombines with core mode at position C which is nearest to the fiber core. Therefore, the accumulated phase difference between the radiated ray and core mode is expressed as

$$\Delta P = 2\pi n_2 \frac{L_1 + L_2}{\lambda} + \phi_r - Z\beta \tag{2}$$

where $L_1$, $L_2$, and $Z$ are the lengths of line AB, line BC, and arc AC on the effective bend radius $R_{eff}$, respectively; $n_2$, $\lambda$, and $\beta$ are cladding RI, wavelength in free space, and propagation constant of

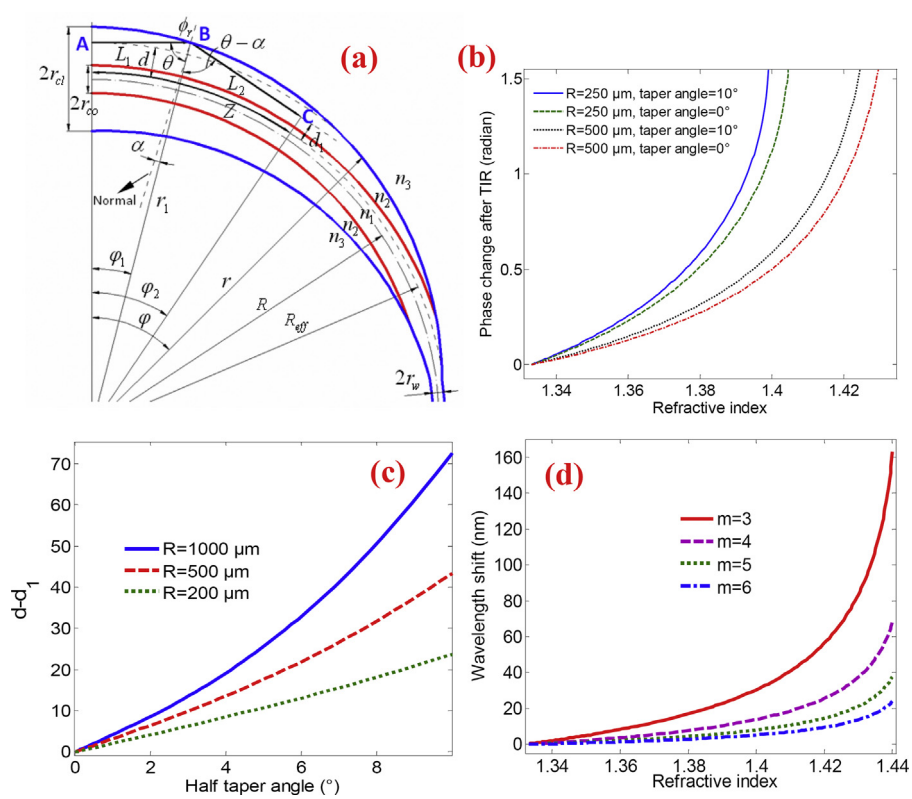


**Fig. 2.** (a) Parameters for modeling the bent downtaper. (b) Calculated phase change after total internal reflection ($\phi_r$ in (a)) versus external RI. (c) Calculated $d - d_1$ versus half taper angle when $n_3 = 1.4$. (d) Calculated wavelength shift versus external RI.

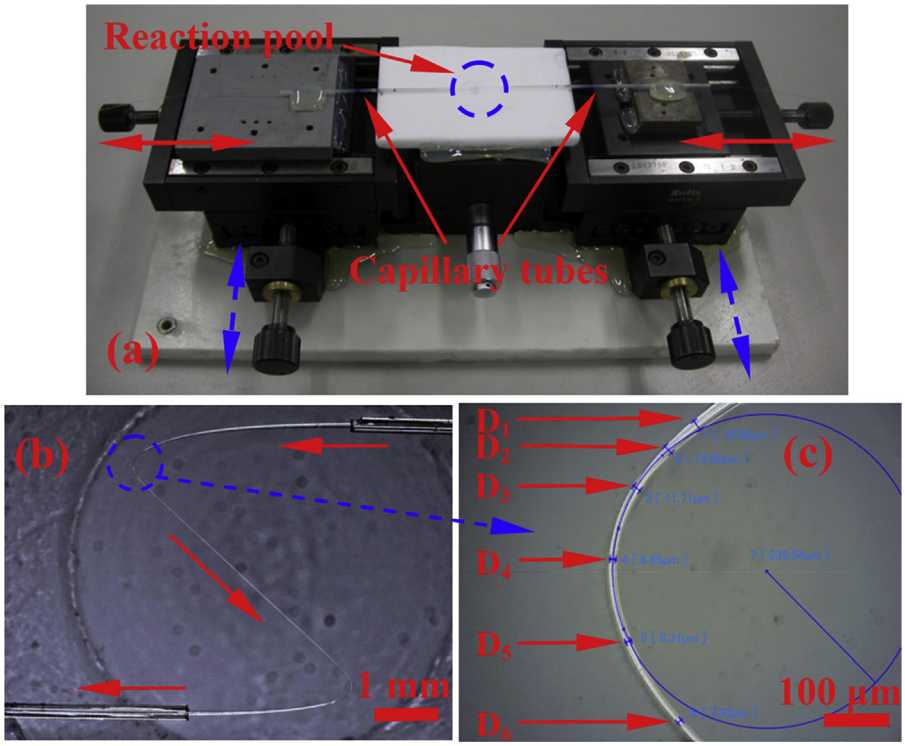


**Fig. 3.** (a) Adjusting apparatus for the S-TOF. (b) Optical microscope image of one S-TOF. (c) Enlarged view of the bent downtaper. The measured diameters of $D_1$, $D_2$, $D_3$, $D_4$, $D_5$, and $D_6$ are 16.62, 14.00, 11.71, 8.65, 8.31, and 7.33 μm, respectively, and the minimum bend radius is ~239.54 μm.

core mode, respectively; $\phi_r$ is the phase change after TIR and given as

$$\phi_r = -2\tan^{-1}\left(\frac{\sqrt{n_2^2\sin^2\theta - n_3^2}}{n_2\cos\theta}\right) \quad (3)$$

for TE polarization, where $\theta$ and $n_3$ are incident angle and external RI, respectively. The value for TM polarization is close to that of TE polarization when $\theta$ is close to 90° and is thus not provided for simplicity.

### 2.3. Calculated results

When the accumulated phase difference $\Delta P$ equals $2m\pi$ ($m$ is an integer), the radiated field will constructively interfere with core mode and contributes to a series of peaks in the

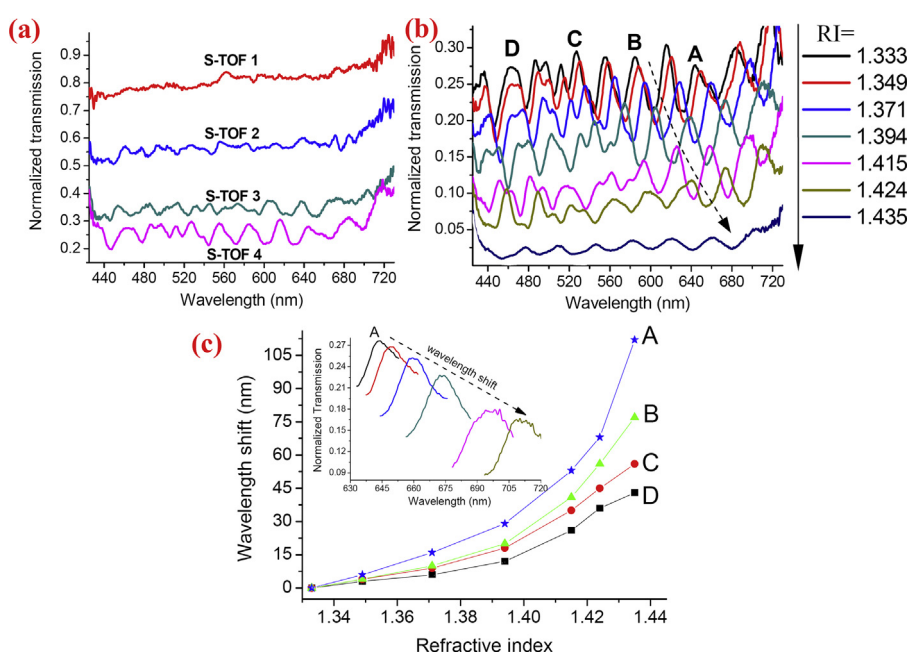


**Fig. 4.** Normalized transmission spectra of (a) the S-TOF during adjusting and (b) the S-TOF 4 immersed in different refractive indices. The dashed arrow designates shift of the resonant peak B as RI increases. (c) Wavelength shift against external RI for peaks A, B, C, and D, inset shows the enlarged view of wavelength shift for peak A.

transmission spectrum. The peak wavelengths shift as external RI varies due to the phase change $\phi_r$ upon TIR of the WGM. In the presence of tapered cladding, the incident angle of TIR will be decreased due to a bias angle of $\alpha$ shown in Fig. 2(a). Using these values $n_1 = 1.462$, $n_2 = 1.457$, $r_{co} = 4.1\,\mu m$, $r_{cl} = 10\,\mu m$, and $\lambda = 633$ nm, the calculated results are plotted in Fig. 2(b) and (c). In Fig. 2(b), the phase change $\phi_r$ of TE polarization versus external RI $n_3$ is plotted for the taper angle of 10° and 0° (i.e., with uniform cladding) with different bend radii. One the one hand, the taper angle accelerates the phase change and thus makes the wavelength shift more sensitive to RI change, the sensitivity enhancement could be more pronounced if the incident angle is further decreased to approach the critical angle. The decreased bend radius also helps to accelerate the phase variation and enhance the sensitivity. One the other hand, due to the tapered cladding, the reflected ray propagates more closely toward the fiber core ($d_1$ in Fig. 2(a)) compared to its original radiation position ($d$ in Fig. 2(a)) as shown by the difference between $d$ and $d_1$ against half taper angle for different bend radii in Fig. 2(c), resulting in a stronger coupling between the WGM and core mode. The enhanced coupling is responsible for the clearer peaks in the transmission spectra.

The calculated wavelength shift (according to the experimental parameters of the BOFT shown in Fig. 3(c)) versus external RI is plotted in Fig. 2(d), which suggests that the peaks red shift when RI increases. The m values of 3, 4, 5, and 6 correspond to peak wavelengths of 1034, 777.5, 623.7, and 521.1 nm, respectively, when external RI is 1.333. It indicates that higher sensitivity is obtained at longer wavelength.

## 3. Experiment and discussion

### 3.1. Adjusting apparatus

A straight tapered optical fiber was fabricated by chemical etching using hydrofluoric acid, then the BOFT was formed by bending the straight tapered fiber on the adjusting apparatus as shown in Fig. 3(a), where two red solid double-head arrows designate the adjusting directions to form displacements along the fiber axis and the other two blue dashed double-head arrows designate the directions to adjust lateral displacements. Two capillary tubes were used to fix both ends of the tapered fiber to facilitate adjustments. However, the adjustments produced an 'S'-like tapered optical fiber (S-TOF) as exhibited in Fig. 3 (b) in which the solid red arrows denote directions of light propagation. Obviously, the S-TOF which was formed due to the mechanical tension and could be flexibly manipulated had two bent regions, one was the bent downtaper and the other was the bent uptaper. Close view of the bent downtaper is shown in Fig. 3(c). The cladding was completely removed where the diameter was less than 8.2 μm (original core diameter of SMF-28e, Corning), thus the bending occurred well within the region with residual tapered cladding.

### 3.2. Results and discussion

The tapered fiber shown in Fig. 3(b) had a length of 6 mm and a waist diameter of 6.1 μm which meant its cladding in the waist section was completely removed. Output spectrum of the straight tapered fiber in water was recorded for the use of normalization. The two capillary tubes were first moved against each other both with an axial displacement of 4.8 mm, after which the lateral movement was exerted to form the S-TOF configuration. The larger the lateral displacement, the more bend loss and thus lower overall transmission as shown in Fig. 4(a), S-TOF 1, 2, 3, and 4 correspond to a lateral displacement of 0.9, 3.15, 4.05, and 4.5 mm, respectively. For S-TOF 1, the bent region was not within the cladded taper, therefore, no oscillations occurred due to no WGMs

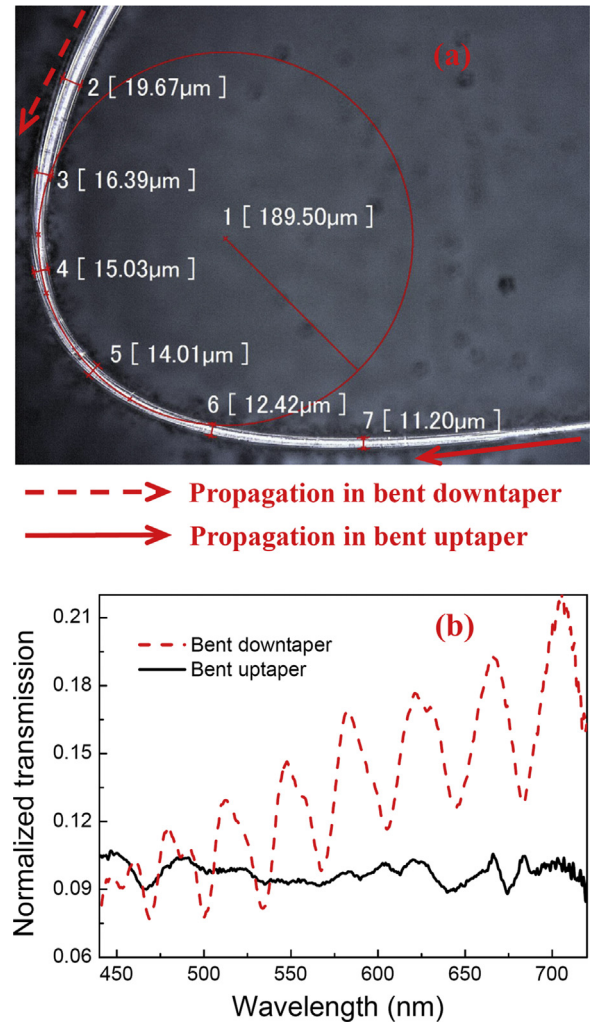


**Fig. 5.** (a) The optical microscope image of a bent optical fiber taper. The dashed and solid arrows denote the propagation directions of light in bent downtaper and uptaper, respectively. (b) The output spectra corresponding to the bent downtaper (dashed, red) and uptaper (solid, black).

without cladding. As the bent region was moved toward cladded taper by increasing lateral displacement, oscillation became more and more clear. The S-TOF 4 whose bent section was well within the cladded taper (Fig. 3(c)) exhibited obvious oscillations in the output spectrum, and the results of S-TOF 4 used for measuring RI are shown in Fig. 4(b). During the RI measurements, the temperature was kept constant at room temperature of circa 20°. There are several peaks over the wavelength range of 430-720 nm, and they all red shift as the external RI increases. The resonance peaks are clearer at the longer wavelengths, which is due to stronger radiations and stronger coupling between the WGM and core mode at longer wavelengths. If we denote several peaks as A, B, C, and D in Fig. 4(b), then the wavelength shifts can be easily read for each resonant peak and the results are shown in Fig. 4(C). Notably, resonant peak at longer wavelength (see peak A) shows higher sensitivity compared to resonant peak at shorter wavelength (e.g., peak D), which is consistent with the theoretical predictions. The wavelength shift of circa 44 nm was experimentally obtained for peak A when external RI increased from 1.424 to 1.435, suggesting a high sensitivity of 4000 nm/RIU or a resolution of $2.5 \times 10^{-6}$ RIU assuming a 10-pm wavelength shift can be distinguished.

The calculated (Fig. 2(d)) and experimental (Fig. 4(c)) results are consistent in these two aspects: one is that peak wavelength red shifts as RI increases, the other is that longer wavelength

results in higher sensitivity. However, due to the practical complexity of taper profile and bending deformation, the experimentally obtained wavelength shifts are not precisely predicted by the simplified theoretical model.

As aforementioned, there is also a bent uptaper in the adjusted S-TOF (Fig. 3(b)). However, compared to the bent downtaper which has been theoretically analyzed in the theory part, the bent uptaper contributes little to the performance because it has the opposite effects in terms of the incident angle of TIR and coupling between the WGM and core mode, i.e., the incident angle is increased and the reflected ray deviates from the fiber core. In order to provide practical visions, an experiment was carried out. In the experiment, only one BOFT was formed as shown in Fig. 5(a), the BOFT played the role of bent downtaper/uptaper when light was propagated in the direction of dashed/solid arrow. The according output spectra are shown in Fig. 5(b), while the BOFT working as a bent downtaper gave rise to a resonant spectrum (dashed and red curve), the BOFT working as a bent uptaper produced a spectrum without obvious oscillations (solid and black curve). Therefore, the oscillatory spectra shown in Fig. 4(b) should be due to the bent downtaper rather than uptaper of the S-TOF shown in Fig. 3(b). Because it is much easier to form and adjust an S-TOF than only one bent downtaper, the S-TOF structure was applied in the previous experiments.

## 4. Conclusion

In conclusion, a highly sensitive refractometer based on BOFT has been theoretically and experimentally investigated. The tapered cladding of the BOFT decreases the incident angle of TIR of the WGM which is formed along the cladding wall due to radiation from the bent fiber core and thus the phase change is accelerated when external RI varies, leading to an increased wavelength shift. A high sensitivity of 4000 nm/RIU over the RI range of 1.424–1.435 was experimentally obtained. This highly sensitive all-fiber-based RI sensor which features simple structure provides an alternative for practical applications in e.g., chemical and biological industries.

## Acknowledgements

The authors are grateful to financial supports from the National High Technology Research and Development Program (No. 2012AA040503), National Key Foundation (No. 11034007), Natural Science for Youth Foundation of China (No. 61102023), and High Technology Research and Development Program of Jilin Province (No. 20120329).

## References

[1] F. Xu, G. Brambilla, Demonstration of a refractometric sensor based on optical microfiber coil resonator, Applied Physics Letters 92 (2008) 101126.
[2] M. Han, F. Guo, Y. Lu, Optical fiber refractometer based on cladding-mode Bragg grating, Optics Letters 35 (2010) 399–401.
[3] C.-L. Zhao, L. Qi, S. Zhang, Y. Jin, S. Jin, Simultaneous measurement of refractive index and temperature based on a partial cone-shaped FBG, Sensors and Actuators B 178 (2013) 96–100.
[4] Q. Wu, Y. Semenova, B. Yan, Y. Ma, P. Wang, C. Yu, G. Farrell, Fiber refractometer based on a fiber Bragg grating and single-mode-multimode-single-mode fiber structure, Optics Letters 36 (2011) 2197–2199.
[5] Q. Wang, G. Farrell, All-fiber multimode-interference-based refractometer sensor: proposal and design, Optics Letters 31 (2006) 317–319.
[6] P. Polynkin, A. Polynkin, N. Peyghambarian, M. Mansuripur, Evanescent field-based optical fiber sensing device for measuring the refractive index of liquids in microfluidic channels, Optics Letters 30 (2005) 1273–1275.
[7] O. Frazão, P. Caldas, J.L. Santos, P.V.S. Marques, C. Turck, D.J. Lougnot, O. Soppera, Fabry–Perot refractometer based on an end-of-fiber polymer tip, Optics Letters 34 (2009) 2474–2476.
[8] G. Liu, Y. Wu, K. Li, P. Hao, P. Zhang, M. Xuan, Mie scattering-enhanced fiber-optic refractometer, IEEE Photonics Technology Letters 24 (2012) 658–660.
[9] P. Wang, G. Brambilla, M. Ding, Y. Semenova, Q. Wu, G. Farrell, High-sensitivity, evanescent field refractometric sensor based on a tapered, multimode fiber interference, Optics Letters 36 (2011) 2233–2235.
[10] C.R. Liao, D.N. Wang, X. He, M.W. Yang, Twisted optical microfibers for refractive index sensing, IEEE Photonics Technology Letters 23 (2011) 848–850.
[11] G. Salceda-Delgado, D. Monzon-Hernandez, A. Martinez-Rios, G.A. Cardenas-Sevilla, J. Villatoro, Optical microfiber mode interferometer for temperature-independent refractometric sensing, Optics Letters 37 (2012) 1974–1976.
[12] D. Marcuse, Curvature loss formula for optical fibers, Journal of the Optical Society of America B 66 (1976) 216–240.
[13] Y. Murakami, H. Tsuchiya, Bending losses of coated single-mode optical fibers, IEEE Journal of Quantum Electronics 14 (1978) 495–501.
[14] A.J. Harris, P.F. Castle, Bend loss measurements on high numerical aperture single-mode fibers as a function of wavelength and bend radius, Journal of Lightwave Technology 4 (1986) 34–40.
[15] R. Morgan, J.S. Barton, P.G. Harper, J.D.C. Jones, Wavelength dependence of bending loss in monomode optical fibers: effect of the fiber buffer coating, Optics Letters 15 (1990) 947–949.
[16] Q. Wang, G. Farrell, T. Freir, Theoretical and experimental investigations of macro-bend losses for standard single mode fibers, Optics Express 13 (2005) 4476–4484.
[17] L.C. Bobb, P.M. Shankar, H.D. Krumboltz, Bending effects in biconically tapered single-mode fibers, Journal of Lightwave Technology 8 (1990) 1084–1090.
[18] S.K. Khijwania, B.D. Gupta, Fiber optic evanescent field absorption sensor: effect of fiber parameters and geometry of the probe, Optical and Quantum Electronics 28 (1999) 625–636.
[19] Q. Wang, G. Farrell, T. Freir, G. Rajan, P. Wang, Low-cost wavelength measurement based on a macrobending single-mode fiber, Optics Letters 31 (2006) 1785–1787.
[20] P. Wang, Y. Semenova, Q. Wu, G. Farrell, A fiber-optic voltage sensor based on macrobending structure, Optics and Laser Technology 43 (2011) 922–925.
[21] P. Wang, Y. Semenova, Q. Wu, G. Farrell, Y. Ti, J. Zhang, Macrobending single-mode fiber-based refractometer, Applied Optics 48 (2009) 6044–6049.
[22] A. Iadicicco, D. Paladino, S. Campopiano, W.J. Bock, A. Cutolo, A. Cusano, Evanescent wave sensor based on permanently bent single mode optical fiber, Sensors and Actuators B 155 (2011) 903–908.
[23] S.H. Nam, Whispering Gallery Mode and Cladding Mode Resonance in Optical Fibers in College of Engineering, The Pennsylvania State University, Central County, 2005.
[24] R. Yang, Y.-S. Yu, Y. Xue, C. Chen, Q.-D. Chen, H.-B. Sun, Single S-tapered fiber Mach–Zehnder interferometers, Optics Letters 36 (2011) 4482–4484.
[25] R. Yang, Y.-S. Yu, C. Chen, Y. Xue, X.-L. Zhang, J.-C. Guo, C. Wang, F. Zhu, B.-L. Zhang, Q.-D. Chen, H.-B. Sun, S-tapered fiber sensors for highly sensitive measurement of refractive index and axial strain, Journal of Lightwave Technology 30 (2012) 3126–3132.